Up-conversion superfluorescence induced by abrupt truncation of coherent field and plasmonic nanocavity

doi: https://doi.org/10.1063/1.5128020

The Journal of Chemical Physics

Up-conversion superfluorescence induced by abrupt truncation of coherent field and plasmonic nanocavity

Cite as: J. Chem. Phys. **151**, 224307 (2019); https://doi.org/10.1063/1.5128020
Submitted: 15 September 2019 . Accepted: 27 November 2019 . Published Online: 11 December 2019

Ryosuke Hata, Nobuhiko Yokoshi, Hiroshi Ajiki, and Hajime Ishihara

The Journal of Chemical Physics ARTICLE scitation.org/journal/jcp

Up-conversion superfluorescence induced by abrupt truncation of coherent field and plasmonic nanocavity

Cite as: J. Chem. Phys. 151, 224307 (2019); doi: 10.1063/1.5128020
Submitted: 15 September 2019 • Accepted: 27 November 2019 •
Published Online: 11 December 2019

Ryosuke Hata,[1] Nobuhiko Yokoshi,[1] Hiroshi Ajiki,[2] and Hajime Ishihara[1,3,a)]

AFFILIATIONS

[1] Department of Physics and Electronics, Osaka Prefecture University, Sakai 599-8531, Japan
[2] Department of Science and Engineering, Tokyo Denki University, Saitama 350-0394, Japan
[3] Department of Materials Engineering Science, Osaka University, Toyonaka, Osaka 560-8531, Japan

Note: This paper is part of the JCP Special Topic on Emerging Directions in Plasmonics.
[a)] **Electronic mail:** ishi@mp.es.osaka-u.ac.jp

ABSTRACT

We theoretically propose a new method for generating up-converted coherent light from two-level systems (TLSs) coupled with a plasmonic nanocavity. The emission spectrum of a TLS excited by a strong laser exhibits a triplet structure called the Mollow triplet. If the lower Mollow sideband is tuned to the cavity mode energy, population inversion of a TLS occurs. When the driving laser is abruptly truncated under this condition, an up-converted photon is emitted from the TLSs. We also predict the up-converted superfluorescence from an ensemble of TLSs as a correlation effect among the excited states of the TLSs.

I. INTRODUCTION

Multiparticle correlation of quantum two-level systems (TLSs), such as molecular dyes and quantum dots, is of utmost importance in developing new functions of quantum complex systems.[1] Because the interparticle correlation is caused by the photon exchange among the TLSs,[2] the control of light frequency, intensity, and its spatial structure makes it possible to enhance the correlation effects.

One of the multiparticle correlation effects is the superfluorescense from a dense ensemble of population-inverted TLSs,[3–7] in which a delayed burst of photoemission occurs due to the phase synchronization of the transition dipole of each TLS, i.e., the formation of macroscopic polarization. Although the excited TLSs are initially uncorrelated, the correlation among them is spontaneously developed by emitting and absorbing photons repeatedly. The superfluorescense has been experimentally observed for atomic (molecular) gases,[8–11] solid crystals,[12–14] quantum wells,[15,16] and quantum dots.[17,18]

In this paper, we propose a new method to realize superfluoresence having higher frequency than that of the input laser, i.e., up-converted superfluorescense by using TLSs coupled with a plasmonic nanocavity. The up-conversion of photon frequency is one of the crucial techniques for quantum information technologies because the standard telecommunication wavelength is usually different from that in quantum information processing. The up-converted superfluorescense is achieved by a rapid truncation of the red-detuned driving laser under the population inversion condition of the TLSs. In this sense, this setup is different from those in the previous theoretical studies.[19–21]

This paper is organized as follows: In Sec. II, the method to generate up-converted photons using the plasmonic nanocavity is described with a model Hamiltonian and master equation. In Sec. III, after discussing the calculated results of the up-converted photoemission from the system with a single TLS, we demonstrate the up-converted superfluorescence from the system with an ensemble of TLSs. The up-converted superfluorescence occurs due to the formation of a multiparticle correlation of the TLSs in a photon field designed by localized plasmonic resonance. This up-converted superfluorescence may lead to innovative metrology and energy conversion systems.

II. MODEL AND CALCULATION METHOD

We consider a model system where N TLSs are placed in a plasmonic nanocavity. The plasmonic nanocavity consists of nanoscale metal structures, in which an extremely strong and localized electric field appears due to the localized surface plasmons. This localized field is so enhanced that nonlinear photoexcitations, even in molecules, can be achieved even if a weak field is irradiated.[22,23] Furthermore, it has been proposed that the use of the higher-order modes of localized surface plasmons and hybrid metal–dielectric systems realizes high-Q cavity modes.[24,25]

A pump cw laser with frequency ω_d is directly irradiated, not through the cavity mode with frequency $\hbar\omega_c$, to the TLSs with resonant excitation energy $\hbar\omega_A$ [see Fig. 1(a)]. The interaction between the pump field and TLSs is denoted by $\hbar\Omega(t)$, in which the time dependence comes from the rapid truncation of the pump field. On the other hand, the coupling energy $\hbar g$ between a TLS and a cavity mode photon is constant.

In the rotation wave approximation (RWA), the Hamiltonian of this system is given by

$$\mathcal{H} = \sum_{j=1}^{N} \hbar\Delta\sigma_{j+}\sigma_{j-} + \frac{\hbar\Omega(t)}{2}(J_+ + J_-) + \hbar\delta a^\dagger a + \hbar g(J_+ a + J_- a^\dagger), \quad (1)$$

in the rotational frame of the driving frequency ω_d, where $\Delta = \omega_A - \omega_d$ and $\delta = \omega_c - \omega_d$ are the frequency detunings, $\sigma_{j\pm}$ is the ladder operator of the jth TLS, $J_\pm \equiv \sum_{j=1}^{N} \sigma_{j\pm}$ is the collective ladder operator of the ensemble of the TLSs, and a is the annihilation operator of the cavity mode. The laser frequency ω_d is red detuned from the resonant frequency ω_A of the TLSs, i.e., $\Delta > 0$. The irradiated laser intensity is constant, and the corresponding interaction energy is denoted by $\hbar\Omega_0$.

The irradiation of a strong laser field on to a TLS forms dressed states, and the fluorescence spectra due to the level transitions exhibit a Mollow triplet with peak frequencies of ω_d and $\omega_d \pm \sqrt{\Delta^2 + \Omega_0^2}$.[40] When the lower Mollow frequency is tuned to the cavity mode, i.e., $\delta = -\sqrt{\Delta^2 + \Omega_0^2}$, the maximum population inversion of the TLSs occurs in this system.[33] Such a stationary inversion of TLSs by red-detuned lasers has been theoretically studied.[19–21,33–39] The schematic level diagram of our system is illustrated in Fig. 1(c).

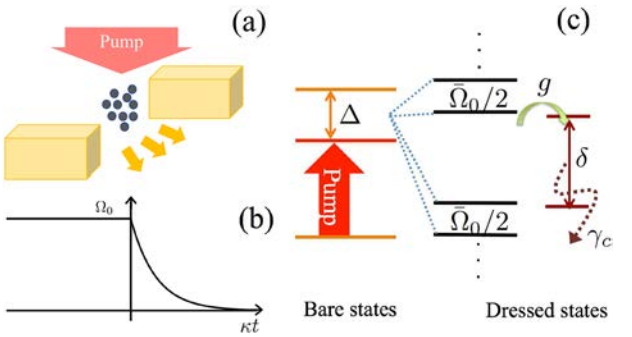

FIG. 1. (a) Schematic picture of an ensemble of TLSs in the bad-cavity limit. (b) Temporal profile of the pump light intensity. (c) Level diagrams for the undressed states and dressed states. Δ and δ denote the TLS detuning and cavity detuning from the driving frequency, respectively. $\bar{\Omega}_0 = \sqrt{\Delta^2 + \Omega_0^2}$ and $\gamma_c = g^2/\kappa$ are the Rabi splitting energy at $t = 0$ and the cavity-modified decay rate of the TLS, respectively.

After achieving the maximum population inversion, the pump laser is rapidly truncated at $t = 0$ with

$$\Omega(t) = \Omega_0[1 - \Theta(t)(1 - e^{-\Gamma t})], \quad (2)$$

where Γ is the truncation rate and $\Theta(t)$ is the Heaviside function [see Fig. 1(b)]. The rapid truncation of the laser results in rapid shrinkage of the level splittings of the Mollow triplet, and therefore, the excited-state population cannot follow the change adiabatically. Owing to this nonadiabatic change, the populations of the TLSs are still inverted after the laser truncation. As a result, the up-converted photons can be emitted from the undressed TLSs.

In the truncation process of the cw laser, the laser frequency is broadened in the order of $1/\Gamma$. This effect partly assists the excitation of the TLSs. In order to reduce the broadening effect on the excitation, we restricted the truncation rate $\Gamma \lesssim \Delta/2$ in the following calculations. The frequency broadening is considered to be much smaller than the excitation frequency ω_A of the TLSs; therefore, the RWA is valid in our system.

The dissipation effects of the cavity photons and the excited states of the TLSs are introduced using the master equation. Here, we consider the bad-cavity limit in which the dissipation rate κ of the cavity photons is much larger than the interaction g between a cavity photon and a TLS. Furthermore, we assume that g is much larger than the dissipation rate γ of the TLSs. Under the condition $\kappa \gg g \gg \gamma$, the cavity-mode variable can be adiabatically eliminated, and therefore, only the operators of the TLSs appear in the master equation. This cavity-modified master equation in the bad-cavity limit was first derived by Zhou.[20] By using this procedure, we extend the cavity-modified master equation to the case of multiple TLSs. The resultant master equation for the density matrix ρ is written as

$$\frac{d}{dt}\rho(t) = -\frac{i}{\hbar}[\mathcal{H}_A, \rho(t)] + \mathcal{L}_A\rho(t) + \mathcal{L}_{cm}\rho(t), \quad (3)$$

where

$$\mathcal{L}_A\rho(t) = \gamma(2J_-\rho(t)J_+ - J_+J_-\rho(t) - \rho(t)J_+J_-), \quad (4)$$

and

$$\mathcal{L}_{cm}\rho(t) = \gamma_c \sum_{j=1}^{N} \{J_-\rho(t)S_{j+}(t) + S_{j-}(t)\rho(t)J_+ - J_+S_{j-}(t)\rho(t) - \rho(t)S_{j+}(t)J_-\}, \quad (5)$$

are the Lindblad superoperators. In Eq. (5), $\gamma_c = g^2/\kappa$ is the photoemission rate of the TLSs, and $S_{j-}(t) = \mathcal{A}_0(t)\sigma_{jz} + \mathcal{A}_1(t)\sigma_{j+} + \mathcal{A}_2(t)\sigma_{j-}$ is the cavity-modified lowering operator; the lengthy expressions of $\mathcal{A}_i(t)$ are given in Appendix A.

To solve the infinite hierarchy of the Heisenberg equations, we employ the cluster expansion method in which the higher-order expectation values are approximately derived using the products

of the expectation values at a certain order.[26–28] In particular, we employ the formulation presented by Leymann *et al.*[29–31] In the formulation, the system dynamics are reduced to four equations of motion for $\langle\sigma_{1-}\rangle$, $\langle\sigma_{1z}\rangle$, $\langle\sigma_{1+}\sigma_{2-}\rangle$, and $\langle\sigma_{1-}\sigma_{2-}\rangle$ in a closed form, where $\langle\sigma_{i+}\sigma_{i-}\rangle = \langle\sigma_{1+}\sigma_{1-}\rangle$ and $\langle\sigma_{i\pm}\sigma_{j-}\rangle = \langle\sigma_{1\pm}\sigma_{2-}\rangle$ $(i \neq j)$ are derived from the symmetric properties of these expectation values. The explicit forms of these equations are shown in Appendix B.

The equations of motion describe the population and emitted photon dynamics after the truncation of the incident laser. According to the input-output theory, the annihilation operator of the emitted photons is given by $a_{\rm out} = \sum_{i=1}^{N}\sqrt{\gamma}\sigma_{i-}$,[32] and hence, the emitted photon number is given by

$$\langle a_{\rm out}^{\dagger}a_{\rm out}\rangle = \gamma N\langle\sigma_{1+}\sigma_{1-}\rangle + \gamma N(N-1)\langle\sigma_{1+}\sigma_{2-}\rangle. \tag{6}$$

The second term represents the cooperative effect of photoemission. The inter-TLS correlation $\langle\sigma_{i+}\sigma_{j-}\rangle$ $(i \neq j)$ is enhanced by increasing the inter-TLS interaction through an increase in Ω_0. The photoemission spectra $S(\omega)$ measured after the laser truncation is calculated from

$$S(\omega) = \sum_{j=1}^{N}\left\langle\left|\int_{-\infty}^{\infty}dt\Theta(t)\sqrt{\gamma}\sigma_{j-}e^{-i\omega t}\right|^2\right\rangle. \tag{7}$$

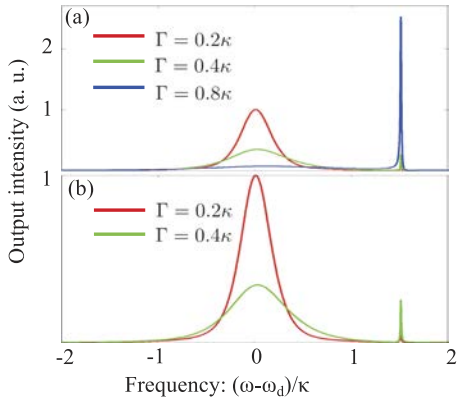

FIG. 2. Photoemission spectra of the cavity system with a single TLS after the truncation of the driving laser with $\omega = \omega_d$ for the truncation rates $\Gamma = 0.2\kappa$, 0.4κ, and 0.8κ in (a). We use the parameters $\Omega_0/\kappa = 5$, $g/\kappa = 0.3$, $\Delta/\kappa = 1.5$, and $\gamma/\kappa = 4.4 \times 10^{-3}$. The Mollow triplet levels of $\omega = \omega_d$ and $\omega_d \pm \sqrt{\Delta^2 + \omega_0^2}$ lie at $(\omega - \omega_d)/\kappa = 0$ and ± 5.22 with the present parameters. The cavity-mode frequency ω_c is tuned to resonance with the lower Mollow triplet. The sharp peak at 1.5 indicates the signal of the up-converted photoemission, which corresponds to the photoemission from the undressed TLS. The intensity of the up-converted photoemission increases with Γ. To clearly see the up-converted sharp peaks for $\Gamma = 0.2\kappa$ and 0.4κ, the range of the vertical axis is changed and the result of $\Gamma = 0.8\kappa$ is eliminated in (b).

III. RESULTS

A. Single TLS

We first demonstrate the up-converted photoemission from a single TLS coupled with a plasmonic nanocavity for various truncation decay rates Γ of the irradiated laser. The photoemission from the stationary driving system, which exhibits a Mollow triplet, is caused by the transitions between the dressed states, that is, the photoemission due to the level transition of an undressed TLS does not occur. However, the photons can be emitted from the undressed TLS when the laser is rapidly truncated. This is because the rapid truncation leads to nonadiabatic level transitions of the TLS.

Figure 2 shows the photoemission spectra of a single TLS for various truncation rates $\Gamma = 0.2\kappa$, 0.4κ, and 0.8κ. For $\kappa = 18$ GHz, the corresponding truncation time is on the order of 100 ps. Since a truncation time of ~100 fs has been obtained,[41] these truncation times are quite feasible. We employ the following parameters in the calculations: $\Omega_0/\kappa = 5$, $g/\kappa = 0.3$, $\Delta/\kappa = 1.5$, and $\gamma/\kappa = 4.4 \times 10^{-3}$. The lower Mollow triplet $(\delta = -\sqrt{\Delta^2 + \Omega_0^2})$ is tuned to the cavity mode frequency ω_c, which is the optimal condition for population inversion. Using these parameters, the population inversion of the TLS occurs with the excited-state population of about 0.6.

For $\Gamma = 0.2\kappa$, the spectrum has a single peak at $\omega = \omega_d$ due to elastic scattering.[39] With an increase in Γ, a sharp peak appears and grows at $(\omega - \omega_d)/\kappa = 1.5 = \Delta/\kappa$, i.e., at $\omega = \omega_d + \Delta = \omega_A$. This fact indicates that the peak is caused by the photoemission from the undressed TLS. The peak frequency is higher than that of the irradiated laser, that is, the peak is a signal of the up-converted photoemission. This peak becomes dominant for $\Gamma = 0.8\kappa$. Note that the peak position is slightly shifted from ω_A because of the cavity-TLS interaction (see Appendix C for details).

B. TLS ensemble

Next, we consider the case of multiple TLSs in the plasmonic nanocavity. The emitted photon number is proportional to N if the TLSs emit photons independently, i.e., only the first term of Eq. (6) is taken into account. The N dependence is eliminated by changing the coupling from g to $\sqrt{N}g$. The second term of Eq. (6) provides a cooperative effect, i.e., a super-linear growth in the emitted photon number. Therefore, if an N dependence appears in the photoemission properties with fixed $\sqrt{N}g$, it represents a cooperative effect on the excitation population and emitted photon dynamics. In the following calculations, we choose $\sqrt{N}g/\kappa = 0.3$. The other parameters are set to be the same as those in the case of a single TLS, and the lower Mollow triplet is tuned to the cavity-mode frequency ω_c as well, as shown in Sec. III A.

Figure 3 shows the photoemission spectra around the up-converted emission peak at $\omega = \omega_A$ for $N = 1$, 5, and 10 with a truncation rate of $\Gamma = 0.8\kappa$. The intensity of each spectrum is normalized by its own peak intensity. It is found that the photoemission linewidth increases with increasing N. This fact indicates that a cooperative effect exhibits super-linear spectral broadening of the up-converted emission peak with increasing N. This is because the radiative decay rate of the TLSs is enhanced by the correlations between different TLSs.

The excited-state populations of the TLSs are calculated as 0.6, 0.533, and 0.495 for $N = 1$, 5, and 10, respectively. For a constant Ω_0 or laser-field intensity, a more intense field is necessary to reach a similar excited-state population per TLS for a larger N.[19]

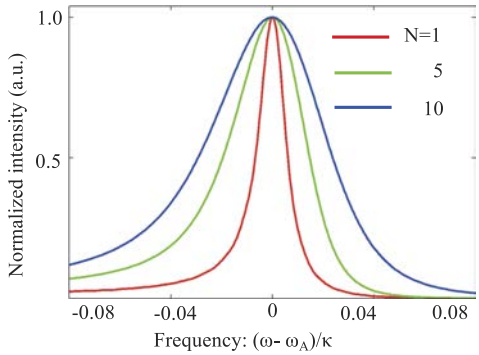

FIG. 3. Photoemission spectrum for various numbers of TLSs, namely, $N = 1$, 5, and 10. The laser truncation rate is $\Gamma = 0.8\kappa$, and the cavity-TLS coupling is $\sqrt{N}g/\kappa = 0.3$. The other parameters are the same as those in Fig. 2. Each spectral intensity is normalized by its own peak intensity.

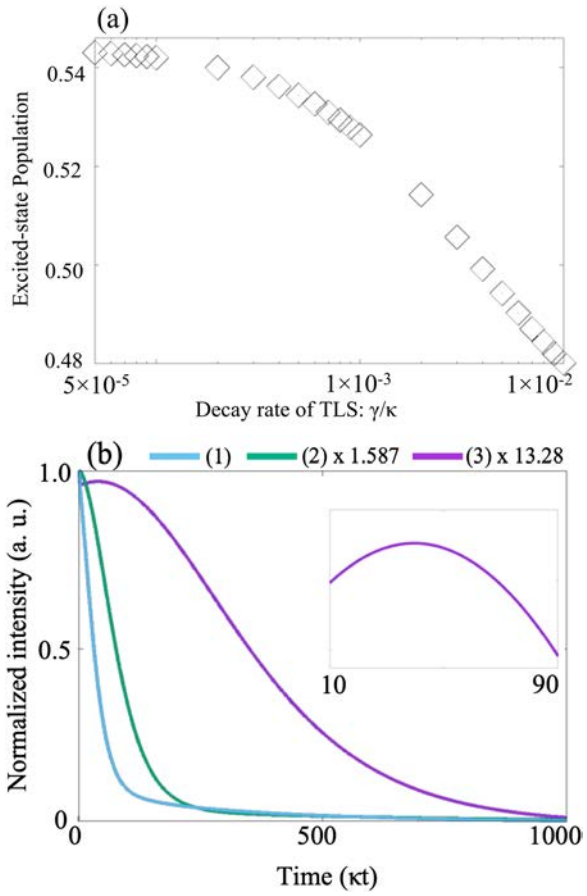

FIG. 4. (a) Excited-state population of a TLS as a function of the decay rate γ of a single TLS. (b) Photoemission dynamics of $N = 10$ TLSs with $\sqrt{10}g/\kappa = 0.3$ for various decay rates γ: (1) $\gamma/\kappa = 5 \times 10^{-3}$, (2) $\gamma/\kappa = 2 \times 10^{-3}$, and (3) $\gamma/\kappa = 2 \times 10^{-4}$. The other parameters are the same as those in Fig. 2. The delayed peak for $\gamma/\kappa = 2 \times 10^{-4}$ is magnified in the inset.

In Fig. 4(a), the populations per TLS for $N = 10$ are shown as a function of the dissipation rate γ of the TLSs. The population increases with decreasing γ and reaches 0.543 in the bad-cavity limit. A larger inverted population can be obtained by using a TLS coupled to an off-resonant cavity in the strong coupling regime[34] or by designing a large deviation of the photonic mode density between the Mollow sidebands.[19]

Figure 4(b) shows the time profiles of the spectral intensity after the laser truncation for various γ calculated from Eq. (6). The intensity is normalized by that for $\gamma/\kappa = 5 \times 10^{-3}$ at $\kappa t = 0$ and each magnification is indicated. The decay of the photoemission intensity becomes slower with decreasing γ. Note that the photoemission peak appears to be delayed from the laser truncation at $t = 0$ for $\gamma/\kappa = 2 \times 10^{-4}$, where the initial population is inverted. The intensity peak is magnified in the inset. This is a characteristic feature of superfluorescence, where the TLSs spontaneously build up their correlation with each other.

The appearance of superfluorescence can be understood in terms of the dynamics of the inter-TLS correlation, which corresponds to the second term of Eq. (6). Indeed, as shown in the equations of motion in Appendix B, the correlation grows positively during population inversion, $\langle\sigma_{1z}\rangle > 0$. The positive growth of the correlation is the essential point in superfluorescence.[3] On the other hand, the correlation becomes negative for $\langle\sigma_{1z}\rangle < 0$, i.e., the excited population is less than 0.5.

IV. CONCLUSION

We proposed a method to generate up-converted coherent light by rapidly truncating an applied laser. It was found that instead of a steady-state photoemission from the Mollow triplet, the rapid truncation of the light intensity induces an up-conversion superfluorescence from the TLS ensembles with population inversion, which opens a new avenue to realize up-converted coherent light sources. We restrict ourselves to the weak coupling regime in this study. However, the excited-state population can be further enhanced in a strong coupling regime, thus leading to clearer superfluorescence.[34] Finally, it should be remarked that the present theoretical proposal can be applied not only to systems with a plasmonic cavity but also to systems with a semiconductor microcavity such as that used in Ref. 42.

ACKNOWLEDGMENTS

The authors thank Manabu Sakai from Osaka Prefecture University for useful discussions. This work was partially supported by JSPS KAKENHI Grant No. JP18H01151 for Scientific Research on (B), Grant No. JP16H06504 Innovative Areas "Nano-Material Optical-Manipulation," and a JSPS Research Fellow Award (No. 1581004400).

APPENDIX A: CAVITY-MODIFIED OPERATOR

Throughout this work, we assume that the system is at the bad-cavity limit ($\kappa \gg g \gg \gamma$). This assumption enables us to trace out the cavity mode using the cavity parameters. In this case, the cavity-modified density matrix is expressed using the modified operator $S_{j-}(t) = \mathcal{A}_0(t)\sigma_{jz} + \mathcal{A}_1(t)\sigma_{j+} + \mathcal{A}_2(t)\sigma_{j-}$ (see the detailed calculations in Ref. 20). After straightforward calculations, one can find the explicit form of the time-dependent coefficients as follows:

$$\mathcal{A}_0(t) = -\frac{\kappa}{2}\Big[\cos 2\theta(t)\int_0^t d\tau \sin 2\theta(t-\tau)e^{(i\delta-\kappa)\tau} - \sin 2\theta(t)\int_0^t d\tau\ \cos^2\theta(t-\tau)e^{-i\int_{t-\tau}^t \tilde{\Omega}(t')dt'+(i\delta-\kappa)\tau} + \sin 2\theta(t)\int_0^t d\tau \sin^2\theta(t-\tau)e^{i\int_{t-\tau}^t \tilde{\Omega}(t')dt'+(i\delta-\kappa)\tau}\Big], \tag{A1}$$

$$\mathcal{A}_1(t) = \kappa\Big[\frac{\sin 2\theta(t)}{2}\int_0^t d\tau\ \sin 2\theta(t-\tau)e^{(i\delta-\kappa)\tau} + \cos^2\theta(t)\int_0^t d\tau\ \cos^2\theta(t-\tau)e^{-i\int_{t-\tau}^t \tilde{\Omega}(t')dt'+(i\delta-\kappa)\tau} + \sin^2\theta(t)\int_0^t d\tau \sin^2\theta(t-\tau)e^{i\int_{t-\tau}^t \tilde{\Omega}(t')dt'+(i\delta-\kappa)\tau}\Big], \tag{A2}$$

$$\mathcal{A}_2(t) = \kappa\Big[\frac{\sin 2\theta(t)}{2}\int_0^t d\tau\ \sin 2\theta(t-\tau)e^{(i\delta-\kappa)\tau} - \sin^2\theta(t)\int_0^t d\tau\ \cos^2\theta(t-\tau)e^{-i\int_{t-\tau}^t \tilde{\Omega}(t')dt'+(i\delta-\kappa)\tau} - \cos^2\theta(t)\int_0^t d\tau \sin^2\theta(t-\tau)e^{i\int_{t-\tau}^t \tilde{\Omega}(t')dt'+(i\delta-\kappa)\tau}\Big]. \tag{A3}$$

Here, we have used the notation $\tilde{\Omega}(t) = \sqrt{\Omega^2(t)+\Delta^2}$ and $\theta(t) = \arctan[\Omega(t)/(\tilde{\Omega}(t)+\Delta)]$.

APPENDIX B: EQUATIONS OF MOTION

Here, we show the explicit form of the derivation of the equations of motion. When a many-body problem involving a large number of particles is considered, many equations of motion must be derived. Higher-order expectation values emerge for each derived equation of motion, up to the given number of particles. In solving such an infinite hierarchy of differential equations, the cluster expansion method is a powerful tool by which the expectation values of more than the desired order are approximated using the products of the expectation values at a certain order.[26–31] The method we employ in this study is the expectation-value-based formulation presented by Leymann *et al.*[29–31]

The analysis of both the output photon intensity and the emitted photon spectrum requires second-order expectation values. Thus, the third- or fourth-order expectation values can be factorized as

$$\langle 3\rangle = \langle 1\rangle\langle 2\rangle - 2\langle 3\rangle_s, \qquad \langle 4\rangle = \langle 2\rangle\langle 2\rangle - 2\langle 4\rangle_s, \tag{B1}$$

where $\langle N\rangle$ is the Nth-order expectation value and the index "s" is the singlet contribution (a multiple of the first-order expectation values: $\langle 3\rangle_s = \langle 1\rangle\langle 1\rangle\langle 1\rangle$ and $\langle 4\rangle_s = \langle 1\rangle\langle 1\rangle\langle 1\rangle\langle 1\rangle$). Each term indicates a sum over all unique expectation values. In addition, the symmetry of the expectation values with respect to the particle exchange reduces the number of expectation values to be calculated. For example, we have $\langle\sigma_{i+}\sigma_{j-}\rangle = \langle\sigma_{1+}\sigma_{2-}\rangle$ and $\langle\sigma_{i+}\sigma_{i-}\sigma_{j-}\rangle = \langle\sigma_{i-}\sigma_{j+}\sigma_{j-}\rangle = \langle\sigma_{1+}\sigma_{1-}\sigma_{2-}\rangle$ for all $i \neq j$. Using these factorizations and symmetrizations, we can obtain the cluster-expansion-based equations of motion,

$$\frac{d}{dt}\langle\sigma_{1-}\rangle \simeq -i\Delta\langle\sigma_{1-}\rangle + i\frac{\Omega(t)}{2}\langle\sigma_{1z}\rangle - \gamma\{1-(N-1)\langle\sigma_{1z}\rangle\}\langle\sigma_{1-}\rangle + \gamma_c\big[\mathcal{A}_0\{1+(N-1)\langle\sigma_{1z}\rangle^2\} + \mathcal{A}_1\{1+(N-1)\langle\sigma_{1z}\rangle\} \times\langle\sigma_{1+}\rangle + \mathcal{A}_2\{-1+(N-1)\langle\sigma_{1z}\rangle\}\langle\sigma_{1-}\rangle\big], \tag{B2}$$

$$\frac{d}{dt}\langle\sigma_{1z}\rangle \simeq -i\Omega(t)(\langle\sigma_{1+}\rangle - \langle\sigma_{1-}\rangle) - 4\gamma\big\{(\langle\sigma_{1z}\rangle+1)/2 + (N-1)\langle\sigma_{1+}\sigma_{2-}\rangle\big\} + 4\gamma_c\mathrm{Re}\big[\mathcal{A}_0^*\{1-(N-1)\langle\sigma_{1z}\rangle\} \times\langle\sigma_{1-}\rangle - \mathcal{A}_1^*(N-1)\langle\sigma_{1-}\sigma_{2-}\rangle - \mathcal{A}_2^*\big\{(\langle\sigma_{1z}\rangle+1)/2 + (N-1)\langle\sigma_{1+}\sigma_{2-}\rangle\big\}\big], \tag{B3}$$

$$\frac{d}{dt}\langle\sigma_{1+}\sigma_{2-}\rangle \simeq \Omega(t)\mathrm{Im}[\langle\sigma_{1z}\rangle\langle\sigma_{1-}\rangle] - 2\gamma\{1-(N-2)\langle\sigma_{1z}\rangle\}\langle\sigma_{1+}\sigma_{2-}\rangle + \gamma\langle\sigma_{1z}\rangle(\langle\sigma_{1z}\rangle+1) + 2\gamma_c\mathrm{Re}\big[\mathcal{A}_0^*\{1-\langle\sigma_{1z}\rangle + (N-2)\langle\sigma_{1z}\rangle^2\}\langle\sigma_{1-}\rangle + \mathcal{A}_1^*\{1+(N-2)\langle\sigma_{1z}\rangle\} \times\langle\sigma_{1-}\sigma_{2-}\rangle + \mathcal{A}_2^*\{-1+(N-2)\langle\sigma_{1z}\rangle\} \times\langle\sigma_{1+}\sigma_{2-}\rangle + \mathcal{A}_2^*\langle\sigma_{1z}\rangle(\langle\sigma_{1z}\rangle+1)/2\big], \tag{B4}$$

$$\frac{d}{dt}\langle\sigma_{1-}\sigma_{2-}\rangle \simeq -2i\Delta\langle\sigma_{1-}\sigma_{2-}\rangle + i\Omega(t)\langle\sigma_{1z}\rangle\langle\sigma_{1-}\rangle - 2\gamma\{1-(N-2) \times\langle\sigma_{1z}\rangle\}\langle\sigma_{1-}\sigma_{2-}\rangle + 2\gamma_c\big[\mathcal{A}_0\{1+\langle\sigma_{1z}\rangle+(N-2)\langle\sigma_{1z}\rangle^2\} \times\langle\sigma_{1-}\rangle + \mathcal{A}_1\{1+(N-2)\langle\sigma_{1z}\rangle\}\langle\sigma_{1+}\sigma_{2-}\rangle + \mathcal{A}_1\langle\sigma_{1z}\rangle \times(1-\langle\sigma_{1z}\rangle)/2+\mathcal{A}_2\{-1+(N-2)\langle\sigma_{1z}\rangle\}\langle\sigma_{1-}\sigma_{2-}\rangle\big]. \tag{B5}$$

Solving these equations yields the population dynamics and the output photon dynamics after the incident light intensity is terminated.

APPENDIX C: SHIFT OF PHOTOEMISSION PEAK FROM UNDRESSED TLS FREQUENCY

The up-converted photoemission peak depicted in Fig. 2 is slightly blue-detuned compared with the undressed TLS frequency owing to the cavity-TLS interaction. Here, we evaluate the shift for zero driving field intensity, $\Omega(t) = 0$, as the field truncation is so rapid that the effect on the eigenfrequencies is negligible. In this case, one can see that $\mathcal{A}_0 = \mathcal{A}_1 = 0$ and $\mathcal{A}_2 = \kappa/[\kappa + i(\delta-\Delta)]$. Substituting these values into Eqs. (B2)–(B5), we obtain the complex frequency of the output light,

$$\omega_{\mathrm{out}} = \Delta - \frac{\gamma_c\kappa(\delta-\Delta)}{\kappa^2-(\delta-\Delta)^2} - i\left(\gamma + \frac{\gamma_c\kappa^2}{\kappa^2-(\delta-\Delta)^2}\right). \tag{C1}$$

The oscillation frequency $\mathrm{Re}[\omega_{\mathrm{out}}]$ is equivalent to the peak in our spectrum calculations for $\Gamma = 0.2\kappa$ and 0.8κ. Thus, we

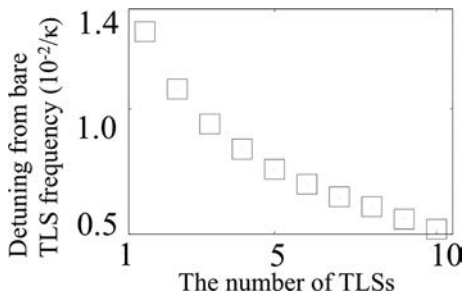

FIG. 5. Numerical computation results for the up-converted peak frequencies detuned from an undressed TLS frequency as functions of N for N = 1–10.

understand that our numerical computation method successfully captures the photoemission spectrum of a single TLS with population inversion.

Our analysis of the photoemission spectrum is also valid for a TLS ensemble. In Fig. 5, the numerically computed peak frequencies differ for different N values because the effective TLS-cavity interaction is changed. Note that in Fig. 3, detuning from the up-converted photoemission peak is depicted in order to ensure visibility for comparison of the linewidth. It is evident from Fig. 5 that increasing the number of TLSs results in a decrease in the eigenfrequency shift. This is because the TLS-cavity interaction is normalized by the square root of N, i.e., $\sqrt{N}g/\kappa$ is fixed.

REFERENCES

[1] M. A. Nielsen and I. Chuang, *Quantum Computation and Quantum Information* (Cambridge University Press, Cambridge, 2000).
[2] K. J. Vahala, Nature **424**, 839 (2003).
[3] R. H. Dicke, Phys. Rev. **93**, 99 (1954).
[4] R. Bonifacio and L. A. Lugiato, Phys. Rev. A **11**, 1507 (1975).
[5] R. Bonifacio and L. A. Lugiato, Phys. Rev. A **12**, 587 (1975).
[6] A. Ishikawa, K. Miyajima, M. Ashida, T. Itoh, and H. Ishihara, J. Phys. Soc. Jpn. **85**, 034703 (2016).
[7] N. Yokoshi, K. Odagiri, A. Ishikawa, and H. Ishihara, Phys. Rev. Lett. **118**, 203601 (2017).
[8] H. M. Gibbs, Q. H. F. Vrehen, and H. M. J. Hikspoors, Phys. Rev. Lett. **39**, 547 (1977).
[9] N. Skribanowitz, I. P. Herman, J. C. MacGillivray, and M. S. Feld, Phys. Rev. Lett. **30**, 309 (1973).
[10] J. Okada, K. Ikeda, and M. Matsuoka, Opt. Commun. **27**, 321 (1978).
[11] G. O. Ariunbold, M. M. Kash, V. A. Sautenkov, H. Li, Y. V. Rostovtsev, G. R. Welch, and M. O. Scully, Phys. Rev. A **82**, 043421 (2010).
[12] R. Florian, L. O. Schwan, and D. Schmid, Phys. Rev. A **29**, 2709 (1984).
[13] M. S. Malcuit, J. J. Maki, D. J. Simkin, and R. W. Boyd, Phys. Rev. Lett. **59**, 1189 (1987).
[14] D. C. Dai and A. P. Monkman, Phys. Rev. B **84**, 115206 (2011).
[15] G. T. Noe II, J.-H. Kim, J. Lee, Y. Wang, A. K. Wójcik, S. A. McGill, D. H. Reitze, A. A. Belyanin, and J. Kono, Nat. Phys. **8**, 219 (2012).
[16] K. Cong, Y. Wang, J.-H. Kim, G. T. Noe II, S. A. McGill, A. Belyanin, and J. Kono, Phys. Rev. B **91**, 235448 (2015).
[17] K. Miyajima, Y. Kagotani, S. Saito, M. Ashida, and T. Itoh, J. Phys.: Condens. Matter **21**, 195802 (2009).
[18] G. Rainò, M. A. Becker, M. I. Bodnarchuk, R. F. Mahrt, M. V. Kovalenko, and T. Stöferle, Nature **563**, 671 (2018).
[19] S. John and T. Quang, Phys. Rev. Lett. **78**, 1888 (1997).
[20] P. Zhou and S. Swain, Phys. Rev. A **58**, 1515 (1998).
[21] H. Takeda and S. John, Phys. Rev. A **83**, 053811 (2011).
[22] K. Ueno, S. Juodkazis, T. Shibuya, Y. Yokota, V. Mizeikis, K. Sasaki, and H. Misawa, J. Am. Chem. Soc. **130**, 6928 (2008).
[23] Y. Osaka, N. Yokoshi, M. Nakatani, and H. Ishihara, Phys. Rev. Lett. **112**, 133601 (2014).
[24] R.-C. Ge, C. Van Vlack, P. Yao, J. F. Young, and S. Hughes, Phys. Rev. B **87**, 205425 (2013).
[25] M. K. Dezfouli, R. Gordon, and S. Hughes, ACS Photon **6**, 1400 (2019).
[26] T. Feldtmann, L. Schneebeli, M. Kira, and S. W. Koch, Phys. Rev. B **73**, 155319 (2006).
[27] M. Kira and S. W. Koch, Prog. Quantum Electron. **30**, 155 (2006).
[28] M. Kira and S. W. Koch, Phys. Rev. A **78**, 022102 (2008).
[29] H. A. M. Leymann, A. Foerster, and J. Wiersig, Phys. Status Solidi C **10**, 1242 (2013).
[30] H. A. M. Leymann, A. Foerster, and J. Wiersig, Phys. Rev. B **89**, 085308 (2014).
[31] H. A. M. Leymann, A. Foerster, F. Jahnke, J. Wiersig, and C. Gies, Phys. Rev. Appl. **4**, 044018 (2015).
[32] D. F. Walls and G. J. Milburn, *Quantum Optics* (Springer-Verlag, Berlin, 1994).
[33] T. Quang and H. Freedhoff, Phys. Rev. A **47**, 2285 (1993).
[34] S. Hughes and H. J. Carmichael, Phys. Rev. Lett. **107**, 193601 (2011).
[35] S. Das and M. A. Macovei, Phys. Rev. B **88**, 125306 (2013).
[36] J. H. Quilter, A. J. Brash, F. Liu, M. Glässl, A. M. Barth, V. M. Axt, A. J. Ramsay, M. S. Skolnick, and A. M. Fox, Phys. Rev. Lett. **114**, 137401 (2015).
[37] R. Manson, K. Roy-Choudhury, and S. Hughes, Phys. Rev. B **93**, 155423 (2016).
[38] M. Nakatani, A. Nobuhiro, N. Yokoshi, and H. Ishihara, Phys. Chem. Chem. Phys. **15**, 8144 (2013).
[39] R. Hata, N. Yokoshi, H. Ajiki, and H. Ishihara, J. Phys. Soc. Jpn. **83**, 093401 (2014).
[40] B. R. Mollow, Phys. Rev. **188**, 1969 (1969).
[41] J. G. Underwood, M. Spanner, M. Yu. Ivanov, J. Mottershead, B. J. Sussman, and A. Stolow, Phys. Rev. Lett. **90**, 223001 (2003).
[42] H. Kim, T. C. Shen, K. Roy-Choudhury, G. S. Solomon, and E. Waks, Phys. Rev. Lett. **113**, 027403 (2014).